2016 IEEE International Conference on Robotics and Automation (ICRA)
Stockholm, Sweden, May 16-21, 2016

sdsdsd

The Second Generation Prototype of A Duct Climbing Tensegrity Robot, DuCTTv2

Jeffrey M. Friesen[1], Paul Glick[1], Michael Fanton[1], Pavlo Manovi[2], Alexander Xydes[3], Thomas Bewley[1], Vytas Sunspiral[4]

***Abstract*— Duct exploration and maintenance is a task well suited for small agile robots, which must be capable of navigating complex and irregular systems of ducts. Previously, we presented a tensegrity robot, DuCTT (Duct Climbing Tetrahedral Tensegrity), which demonstrated the plausibility of such a robot for duct exploration but was never able to successfully demonstrate climbing. Here we present DuCTTv2, redesigned from the ground up to address issues with actuator power, cable routing, compliance and synchronized control present in our first prototype. These improvements allow the prototype to be the first tensegrity robot to demonstrate duct climbing, and does so with an average climb speed of 1.4 cm/s. We also demonstrate initial tests of the prototypes ability to bend and translate its two segments relative to one another, which will allow it to navigate T-junctions and sharp corners commonly found in duct systems. Testing of the prototype is conducted to demonstrate the new faster and more robust control of motion, and analysis of dynamic simulations is presented.**

I. INTRODUCTION

There are many duct systems that are internally inaccessible to humans. The need to repair or explore these systems has driven considerable research towards pipe-climbing robots. These robots must be carefully designed in order to overcome changes in pipe diameter, unexpected obstacles, and abrupt corners within the duct. Current robot designs for duct navigation can be loosely classified into three different locomotion types: wheeled robots, legged robots, and inchworm robots [1].

The majority of duct climbing robots use spring systems to passively wedge wheels between duct walls; while efficient and relatively fast, these robots cannot handle unexpected obstacles or tight turns [2]. Other wheel-based designs employ magnetic wheels to climb up a side of the duct; these designs are better suited for avoiding protruding obstacles, but can be unreliable around sharp turns and only work in metallic pipes [3]. Legged climbing robots are more versatile and can move through more complex systems, although are inefficient in terms of actuation complexity, energy consumption, and weight [2] [1]. There are a variety of pipe-inspection robots that climb via an inchworm type mechanic – the top section is clamped in place, the bottom is raised; the bottom section is clamped in place, the top is raised; and so on [4] [5]. This class of locomotion is suitable for varying pipe sizes and navigation around corners in the ducting, although each step requires sufficient traction and precise spatial positioning [1].

Fig. 1. Render of the DuCTTv2 Prototype. A system of eight independently actuated cables connect two nested tetrahedra to produce complex high degree of freedom motions.

The primary goal of our work is to implement a cable-driven system that creates a compliant tensegrity joint between the wedging elements of such an inchworm robot, thus relaxing requirements on precise spatial positioning through the addition of passive compliance. Tensegrity is a structural design paradigm in which compressive members are separated within a net of tensile members, and some evidence suggests it is also a good model for many biologic structures [6]. By implementing tensegrity principles within our robot we can utilize several key traits that such structures have been

*This work was supported by a NASA Space Technologies Mission Directorate Research Fellowship, NASA's Californian Space Grant Consortium, and also NASA's Human Robotic Systems (HRS) project, Game Changing Developments (GCD) Program, Space Technology Mission Directorate (STMD)

[1]Jeffrey Friesen, Paul Glick, Michael Fanton, and Thomas Bewley are with the UC San Diego Coordinated Robotics Lab, MC 0411, La Jolla CA, 92093 USA jfriesen@ucsd.edu, pglick@ucsd.edu, mfanton@stanford.edu, bewley@ucsd.edu

[2]Pavlo Manovi is with the computer engineering department at UC Santa Cruz 1156 High St, Santa Cruz, CA 95064 me@pavlo.me

[3]Alexander Xydes is a computer science masters student at UC San Diego 9500 Gilman Drive, Mail Code 0404 La Jolla, CA 92093-0404 USA axydes@eng.ucsd.edu

[4]Vytas Sunspiral is a Senior Robotics Researcher, SGT Inc., with the Intelligent Robotics Group, NASA Ames Research Center, Moffett Field CA 94035 USA vytas.sunspiral@nasa.gov

Fig. 2. Image of the DuCTTv2 hardware prototype. The topmost and bottommost rods are linear actuators used for wedging between duct walls. The four hollow vertical aluminum rods of each tetrahedron house batteries and cabling. The two central rods encased in black plastic each house all the needed control circuitry and four BLDC motors for cable actuation.

shown to exhibit including high mass efficiency, system-wide compliance, minimal cross-sectional area, and global external load distribution [7] [8] [9]. However, tensegrity systems are radically different than traditionally structured robots and thus have differing design challenges with less available work of existing solutions.

Because of this, our first prototype, DuCTT [10], experienced frequent mechanical and electrical failures and performed inconsistently even when functional. In this paper we present DuCTTv2, a completely re-engineered tensegrity duct-exploration robot which implements robust solutions to many of the design challenges that small cable-driven robots face. Utilizing the same fundamental topography of our previous prototype, but with vast redesigns of prototype hardware and electronics alongside improvements to control methodology, DuCTTv2 is the first fully functional duct-climbing tensegrity robot.

Additionally, to help establish various design parameters and to test new control strategies, two dynamic simulations are presented and tested. Our new prototype is then evaluated in both simulation and through various physical tests, implying it has all requisite abilities for successful duct navigation. Our approach results in a lightweight system with a simplified mechanical design, which will result in greater reliability and better navigation in uncertain environments.

II. Second Generation Prototype Hardware

The topology of DuCTTv2, two nested tetrahedral structures connected via eight actuated cables, remains unchanged. These tetrahedrons create an over-actuated system which enables six degree of freedom motion. When fully contracted, the entire robot can be packed into a cubic box with sides measuring 40 cm.

With eight, 12-watt maxon BLDC motors and a total system mass of 3.75 kg, DuCTTv2 has a more favorable power to weight ratio than the initial prototype which had six, 1.4-watt motors with a total system mass of 3.1 kg. This 9-fold increase in power density can be attributed to the switch from brushed to brushless DC motors, which are more difficult to use in terms of peripheral circuitry but typically have a much higher power density per volume and weight than brushed alternatives. A 17:1 gear ratio in the vertical cable actuators allows for a theoretical maximum tension of 112 N to be generated while a 67:1 ratio in the saddle cables allows for a maximum tension of 443 N to be applied.

For each tetrahedron, eight Panasonic NCR18650PF batteries are organized in a 4-series 2-parrallel layout to provide a 14.8 volt 6 amp-hour supply capable of safe continuous discharge at 20 amps. Pairs of these batteries reside in the 4 hollow aluminum side tubes of the tetrahedron. Total system current draw during climbing on average falls under 1.5 amps, so the robot can run untethered for over four hours.

Compliance in many cable driven robots is realized through a non-elastic cable in series with an extension spring, or with flexible bungee cables. These methods can introduce problems such as time-dependent stiffness, highly nonlinear stiffness or, plastic deformation under large loading. We have implemented linear compression springs with a stiffness of 4.5 kN/m internal to the structure which avoid such issues with one major benefit being that the springs can fully compress without causing any permanent damage to the spring (see Fig. 3). At 60N the spring experiences its maximum displacement of 1.2cm and the cable experiences a sharp increase in stiffness.

Relative motor position is measured by monitoring hall effect sensors of each BLDC motor. Since the absolute positions will be different depending on motor position during start-up, a calibration routine is implemented. The prototype fully contracts to a locked position in which the tetrahedra are fully nested and the cable lengths are set according to this known configuration.

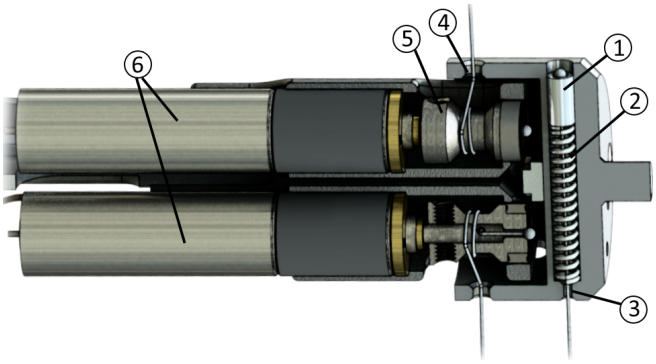

Fig. 3. Cross section of the mid-bar endcap. Two maxon EC motors (6) are attached to cable spools in each of the four end caps. High-modulus polyethylene cables are anchored on one end to a cylindrical metal piston (1), run down the center axis of the compression spring (2) and out the shaft (3) to be threaded into the other tetrahedron's endcap routing hole (4) and anchored to a motor pulley (5).

Improved efficiency has been achieved through simplified cable routing and more efficient gearing. The initial prototype used worm gears in an effort to prevent cable spools from back-driving. This proved to be a major source of friction and DuCTTv2 now uses only planetary gearboxes for mechanical reduction. The cable passes over two bending points when exiting the mid-bar housing and when terminating at the compression springs. Special care was taken to ensure the aluminum eyelet surfaces were rounded and smoothed to prevent snags, and minimize friction and cable-wear.

Each tetrahedron contains a single off-the-shelf lead screw type linear actuator with rubber feet at each end to increase desired static friction between the robot and the walls of duct systems. The actuators change length between 35 and 45 cm, which is the current feasible range for pipe diameter that the prototype can navigate.

III. Embedded System Design

Parallel cable-driven robotic systems often face challenges in temporal synchronisation of control, data acquisition, and distributed communications. From the perspective of pose estimation, distributed communications and sensor data collection can be problematic when values are missed, or there is a non-trivial amount of update jitter [11][12]. DuCTTv2 avoids these pitfalls with tight integration of control circuitry in one set of mating boards which handle: Cable control, commutation of multiple motors, communications, and sensor data acquisition.

While the four BLDC motors per tetrahedron give the robot a large range of motion, they also impose constraints on the embedded system which control the robot. Beyond physical limitations on volume, the use of independent motor controllers per motor would introduce uncertainties in control and sensor data validity, and impose limitations on the types of physical layers used in communications between the motors and the higher level controller. In the interest of minimizing uncertainty in control and sensor results, we developed a BLDC-motor driver board which integrates

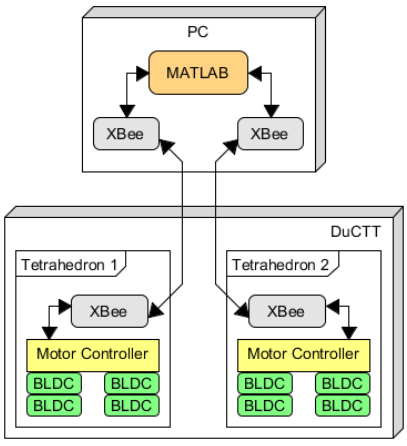

Fig. 4. System communications flow.

current measurement, low-level control, and motor commutation for all four BLDC motors in each tetrahedron. This integration scheme allows for the entire system to operate with only two independent communications nodes, reducing the synchronization requirements to two points per time-step. This demonstrates a great simplification when compared to similar tensegrity structures like that of SUPERBall which has twelve independent nodes which all communicate over a single physical layer.[11]

Cable-length control is achieved through the integration of four BLDC motors, four Texas Instruments DRV8332 MOSFET triple half-bridge modules, and a 16 bit dsPIC33EP256MU810 running at 70 MIPS. In lieu of hardware quadrature encoders, hall effect sensors trigger interrupt requests on the microcontroller which are handled by a software odometry and block commutation routine. Additionally, ADC channels are used to sample the bulk current through each motor to prevent overheating and to infer rough tension estimates.

Controls and communication are separated into high-level and low-level tasks. Each cable has an independent low-level proportional controller to track cable length commands. An external computer then uses a high level inverse-kinematic strategy explained below to generate desired cable-lengths, which are transmitted serially between the dsPIC33E from a PC running matlab over a protocol similar to NMEA-0183 on a IEEE 802.15.4 physical layer through use of xbee modules.

At the time of writing, DuCTTv2's highest level control code is run open loop in MATLAB which sends rest length commands to the motor boards through the 802.15.4 layer at a rate of 50 Hz. Future work will see more advanced embedded processors integrated into the physical prototype to reduce offboard computation requirements.

IV. Dynamic Simulations

Two separate dynamic simulations were created in order to ascertain design requirements for the prototype, test the implementation of various control strategies for the hardware prototypes, and model the interaction of the prototype with the physical environment.

A. Euler Lagrange Simulation

The first simulation generated uses Lagrangian mechanics to obtain the equations of motion. The tetrahedrons mass distribution is modeled using five point masses per tetrahedron, one at each vertex of the tetrahedron and one at the geometric centroid. The state of each tetrahedron is described using Cartesian coordinates, x, y and z, of the central node of each tetrahedron, as well as three Euler angles, θ, γ and ϕ, which are applied using rotation matrices when the central point of the tetrahedron is at the origin, before translations are applied. what is generalized forces ?

Cable forces are applied using generalized forces to handle the piecewise non-linearities associated with unilateral forcing constraints of the cables. Cable forces were initially applied directly at the nodes but were moved to more accurate locations according to the prototype hardware which

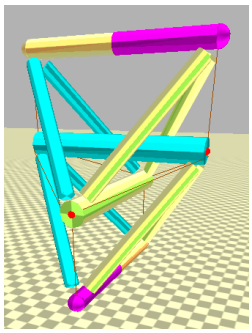

Fig. 5. DuCTT model rendered with NTRT. [16]

we will discuss further below. No collision modeling is performed in this model.

B. NTRT Simulation

The NASA Tensegrity Robotics Toolkit (NTRT) is an open-source library developed by the Intelligent Robotics group at NASA Ames to facilitate simulation of robots based on tensegrity principles [13]. It is built to run on top of the open-source Bullet Physics Engine [14]. The developers have added many tensegrity specific features to the engine, with the goal of creating a reliable engineering tool for the design and control of tensegrity robots. As the native Bullet supplied soft body models were not physically realistic, NTRT has incorporated a custom designed linear cable model using Hooke's law forces to ensure analytic accuracy[15]. Other features include builder tools, motor models, controllers, and machine learning modules. Prior work has validated NTRT against other tensegrity robot hardware implementations[15]. We aim to utilize these features to realistically simulate the robots interaction with itself and the environment, so we constructed a model of DuCTT within NTRT (Fig. 5).

C. Dynamic Simulation Comparison

At the time of writing neither simulation has been validated against the DuCTT hardware due to the requirement of accurate 3D position tracking which was not readily available. However, as a first test, a comparison between the two models was conducted in order to verify that they were in agreement. To accomplish this, we actuated the NTRT model in a controlled manner and recorded the nodal positions and rest length commands applied to the cables at each time step. The same rest length commands were then fed into the Euler-Lagrange model, which was simulated with an identical time step of 1 ms. The six state variables $(x, y, z, \theta, \gamma, \phi)$ of the NTRT model are calculated with a least-squares fit based on the node positions for the model. The node positions and state variables from the two models were then compared.

After the first comparison was performed, the two models were found to be in very poor agreement (Fig. 6, 2cm mounting error). After investigating the possible causes and tweaking many parameters on both models, we determined that the models disagreed due to a discrepancy in cable mount location. Cables were located exactly at the nodes

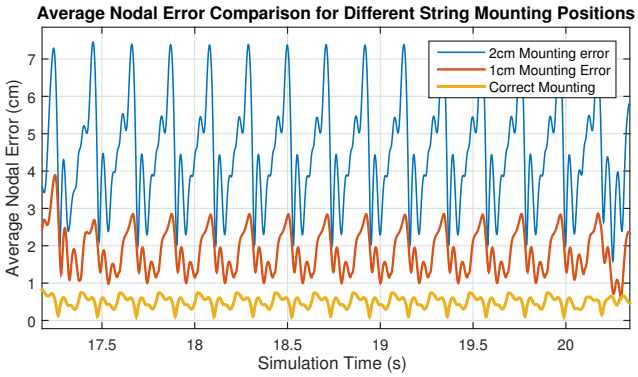

Fig. 6. The average distance between all nodes in the NTRT Simulation and the Euler-Lagrange simulation was calculated for three separate cases. The same NTRT data was kept consistent while the Euler-Lagrange cable mount points were moved from exactly at the nodes, resulting in a 2 cm error, to a bar radius of 2 cm away from the nodes, bringing them into agreement with the NTRT model.

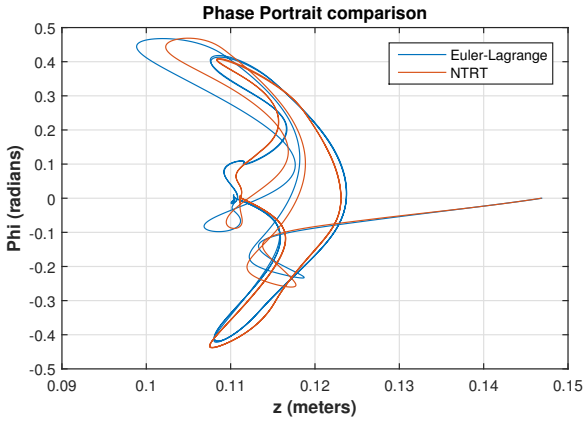

Fig. 7. Phase portrait comparing 2 state variables, corresponding to vertical height and y-axis bending of the tetrahedrons showing a similar path taken through the phase-space. Only two variables are shown here for brevity and clarity but all six state variables were found to be in similar close agreement.

in the Euler Lagrange model but not in the NTRT model which better matched the physical prototype. The results from Fig. 6 demonstrate the importance of accurate cable mount positions. In addition, Fig. 7 shows the similarity in movement between the two models when comparing the y-axis rotation and vertical height after the cable mount locations were corrected in the Euler-Lagrange model.

V. Force Density Method for Inverse Kinematic Control Policy

The work in achieving model agreement between our dynamic simulations indicated that cable mounting locations are critical to model agreement. In order to increase the accuracy of commands generated by our inverse kinematic control policy the cable mounting locations of the model used were moved closer to the physical prototype's geometry. In our first model, sets of cables that mounted to a common rod end were approximated as stemming from a single node allowing the model to have 4 nodes and 6 bars per

tetrahedron. In the new model 8 nodes and 21 bar members per tetrahedron were used to create more accurate cable mount positions.

In our previous paper, [10], we demonstrated the force density method for use in solving the inverse kinematics of a simplified robot model. For a tensegrity system with s cables r bars and n nodes the force density method can be used to pose the problem with a linear set of equations as,

$$\boldsymbol{A}\boldsymbol{q} = \boldsymbol{p}. \tag{1}$$

Where $\boldsymbol{q} \in \mathbb{R}^{s+r}$ is a vector of force densities for all members $\boldsymbol{p} \in \mathbb{R}^{3n}$ are the x, y and z external forces stacked into a single column vector and $\boldsymbol{A} \in \mathbb{R}^{\boldsymbol{3n}\times(\boldsymbol{s+r})}$ is a matrix derived as,

$$\boldsymbol{A} = \begin{bmatrix} \boldsymbol{C}^T diag(\boldsymbol{C}\boldsymbol{z}) \\ \boldsymbol{C}^T diag(\boldsymbol{C}\boldsymbol{y}) \\ \boldsymbol{C}^T diag(\boldsymbol{C}\boldsymbol{z}) \end{bmatrix}, \tag{2}$$

Where $\boldsymbol{C} \in \mathbb{R}^{(s+r)\times n}$ is the connectivity matrix for the given topology and $\boldsymbol{x} \in \mathbb{R}^n$, $\boldsymbol{y} \in \mathbb{R}^n$ and $\boldsymbol{z} \in \mathbb{R}^n$ are vectors containing the desired nodal coordinates. For further elaboration on the details of this method please refer to the following [17] [7]. The Moore-Penrose psuedoinverse can then be used to write the set of solutions to this system as,

$$\begin{bmatrix} \boldsymbol{q}_s \\ \boldsymbol{q}_r \end{bmatrix} = \begin{bmatrix} (\boldsymbol{A}^+)_s \\ (\boldsymbol{A}^+)_r \end{bmatrix} \boldsymbol{p} + \left(\begin{bmatrix} \boldsymbol{I}_s \; 0 \\ 0 \; \boldsymbol{I}_r \end{bmatrix} - \begin{bmatrix} (\boldsymbol{A}^+\boldsymbol{A})_s \\ (\boldsymbol{A}^+\boldsymbol{A})_r \end{bmatrix} \right) \boldsymbol{w} \tag{3}$$

Where the equations have been split between the first s rows and the last r rows to represent which elements contribute to cable force densities and bar force densities where $\boldsymbol{w}$ is a vector of free variables. A cost function should be selected which minimizes the required cable force densities for a given pose but that doesn't incorporate bar force densities. Therefore a straightforward choice is the norm of $\boldsymbol{q}_s$. A constraint must also be placed on $\boldsymbol{q}_s$ to enforce positivity to prevent slack cables. The optimization can then be written as,

$$\begin{aligned} \underset{\boldsymbol{w}}{\text{minimize}} \quad & \boldsymbol{w}^T\boldsymbol{V}^T\boldsymbol{V}\boldsymbol{w} + 2\boldsymbol{w}^T\boldsymbol{V}^T(\boldsymbol{A}^+)_s\boldsymbol{p} \\ \text{subject to} \quad & {}^T(\boldsymbol{A}^+)_s\boldsymbol{p} + \boldsymbol{V}\boldsymbol{w} \geq 0, \end{aligned} \tag{4}$$

Here $\boldsymbol{w}$ represents a vector of free variables to be optimized, whose length corresponds to the number of columns in $\boldsymbol{V}$. Previously we selected $\boldsymbol{V}$ to equal $(\boldsymbol{I} - \boldsymbol{A}^+\boldsymbol{A})_s$ or the first s rows of the matrix which represents the nullspace of $\boldsymbol{A}$. This choice will produce the correct solution but since $\boldsymbol{V}$ would be an s by $(s+r)$ matrix, its rank will be less than or equal to s. By instead reducing $\boldsymbol{V}$ to an orthogonal matrix whose columns are a basis of the original matrix, we simultaneously reduce the number of free variables in the optimization and also enforce that $\boldsymbol{V}^T\boldsymbol{V}$ will be positive-definite, ensuring convexity.

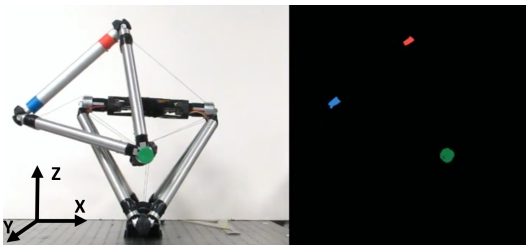

Fig. 8. Colored markers used for tracking the 2-D position of the prototype.

VI. Prototype Testing and Performance Analysis

In order to evaluate the performance of the prototype several different testing scenarios were implemented. Note that during all of these tests motor PWMs were saturated at fourty percent of the maximum possible duty cycle for initial testing, so the robots speed and power are underrepresented in this testing. More intermediate testing and analysis needs to be done to ensure that proper protective measures are in place to prevent over-heating of the motors and enforce that motor velocities remain below the maximum allowable input speeds to the gearboxes before this constraint is lifted.

The first assessment was intended to replicate a test conducted on the first hardware prototype in our prior work [10]. The prototype was filmed at 23 frames-per-second from a fixed position and affixed with colored markers for 2D motion tracking in post-processing (Fig 8). The base tetrahedron was first mounted to an isolation table, then a series of open loop commands for vertical translation and rotation about an axis normal to the camera angle were commanded. A total of 250 commands were sent over the 18 second interval corresponding to an update rate of approximately 14 Hz.

This test illustrates the overall improvements made to actuation speed with the new prototype hardware. Referring to Fig. 9 we can see that, in 9 seconds, the new prototype is able to complete the same series of commands that took the previous prototype 80 seconds to complete.Additionally, no rapid jumps in position are observed as was the case with the previous prototype.

It is shown that the largest Z-position errors of approximately 4cm occur during times of high positive velocity, when the saddle-cable motors lift the tetrahedron vertically. These errors are better viewed temporally, as a delay between motor command and output as the cable lift the upper tetrahedron, and could be addressed through better low level control strategies for the independent cables. The bending actuation is more accurate with errors typically below one degree and maximum errors below four degrees. The bending is primarily controlled by vertical cables which in this orientation experience much lower overall tensions.

The second test conducted was a climb of a straight vertical duct with a diameter of 36 cm and a height of 76 cm. It took the robot 32 seconds to climb this duct section, subtracting the contracted length of the robot This results

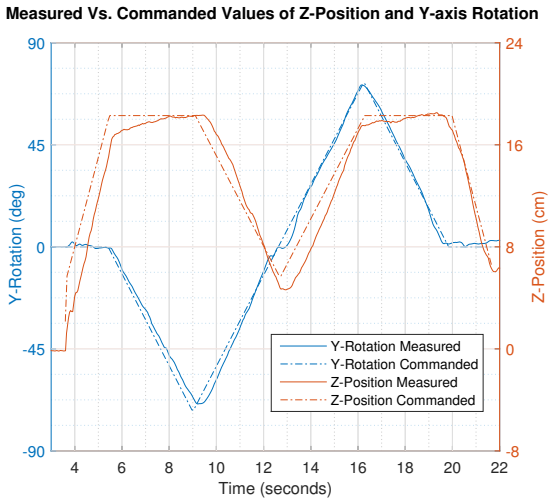

Fig. 9. Dotted lines are commanded angles and positions fed into the inverse-kinematic controller and sent to the robot. Solid lines represent measured values found through post-processing of the video.

in an average climbing speed of 1.4 cm/s. This test was not optimized for speed but instead was purposed as a first demonstration of climbing ability. Since the robot currently spends about 45% of its total climbing time extending and contracting linear actuators to grab and release duct walls and only 55% contracting and extending the cables to ascend, finding a faster modular replacement for the linear actuator, which currently has a maximum speed of 1 cm/s, would yield large gains in climbing speeds.

VII. Future Work

原型

We have shown that the prototype is capable of all requisite abilities for duct climbing and conducted an initial climb of a short duct section. However, the prototype in it's current state requires further testing to fully evaluate and demonstrate its abilities. Climbing commands need to be optimized to ascertain maximum average climb-speed. A test structure needs to be built in order to test the prototype's ability to manage right-angles and T-junctions within duct systems. Increased supervisory control of the BLDC motors needs to be implemented in software to ensure the motors stay within safe operating conditions while still allowing for maximum performance.

Further hardware improvements also need to be made to improve overall performance. Our first priority will be the integration of cable tension sensors, to improve state-estimation and also allow for prevention of slack cables. Secondly, a better linear actuator needs to be purchased or custom-made to improve climbing speed.

Both DuCTT simulations presented here need to be validated against the DuCTT hardware prototype to ensure that the models are adequate. This will make the models more useful in the development of new control strategies, both through machine-learning and analytic methods.

VIII. Acknowledgments

We appreciate the support, ideas, and feedback from members of the Dynamic Tensegrity Robotics Lab: Ken Caluwaerts, Jonathan Bruce, Atil Iscen, In Won Park, and Brian Tietz. We would also like to thank Fiber-Tech Engineering for the donation of small duct samples for climbing tests, and to Tom Chalfant and the MAE Undergraduate Machine Shop for their aid in fabrication. We also appreciate the support from Terry Fong and the Intelligent Robotics Group at NASA Ames Research Center, and the staff of the NASA Ames Space Shop in further enabling DuCTTv2.

References

[1] R. Richardson, S. Whitehead, T. Ng, Z. Hawass, A. Pickering, S. Rhodes, R. Grieve, A. Hildred, A. Nagendran, J. Liu, *et al.*, "The djedi robot exploration of the southern shaft of the queen's chamber in the great pyramid of giza, egypt," *Journal of Field Robotics*, vol. 30, no. 3, pp. 323–348, 2013.

[2] W. Neubauer, "A spider-like robot that climbs vertically in ducts or pipes," in *Intelligent Robots and Systems' 94.'Advanced Robotic Systems and the Real World', IROS'94. Proceedings of the IEEE/RSJ/GI International Conference on*, vol. 2. IEEE, 1994, pp. 1178–1185.

[3] Y. Kawaguchi, I. Yoshida, H. Kurumatani, T. Kikuta, and Y. Yamada, "Internal pipe inspection robot," in *Robotics and Automation, 1995. Proceedings., 1995 IEEE International Conference on*, vol. 1. IEEE, 1995, pp. 857–862.

[4] J. Lim, H. Park, S. Moon, and B. Kim, "Pneumatic robot based on inchworm motion for small diameter pipe inspection," in *Robotics and Biomimetics, 2007. ROBIO 2007. IEEE International Conference on*. IEEE, 2007, pp. 330–335.

[5] W. Jeon, J. Park, I. Kim, Y.-K. Kang, and H. Yang, "Development of high mobility in-pipe inspection robot," in *System Integration (SII), 2011 IEEE/SICE Int. Symposium on*. IEEE, 2011, pp. 479–484.

[6] T. Flemons. (2007) The geometry of anatomy. [Online]. Available: http://www.intensiondesigns. com/geometry of anatomy.html, 2007

[7] R. E. Skelton and M. C. Oliveira, *Tensegrity systems*. Springer, 2009.

[8] R. E. Skelton, R. Adhikari, J.-P. Pinaud, W. Chan, and J. Helton, "An introduction to the mechanics of tensegrity structures," in *Decision and Control, 2001. Proceedings of the 40th IEEE Conference on*, vol. 5. IEEE, 2001, pp. 4254–4259.

[9] C. Paul, F. J. Valero-Cuevas, and H. Lipson, "Design and control of tensegrity robots for locomotion," *Robotics, IEEE Transactions on*, vol. 22, no. 5, pp. 944–957, 2006.

[10] J. Friesen, A. Pogue, T. Bewley, M. de Oliveira, R. Skelton, and V. Sunspiral, "Ductt: A tensegrity robot for exploring duct systems," in *Robotics and Automation (ICRA), 2014 IEEE International Conference on*. IEEE, 2014, pp. 4222–4228.

[11] A. P. Sabelhaus, J. Bruce, K. Caluwaerts, P. Manovi, R. F. Firoozi, S. Dobi, A. M. Agogino, and V. SunSpiral, "System design and locomotion of superball, an untethered tensegrity robot," in *Robotics and Automation (ICRA), 2015 IEEE International Conference on*. IEEE, 2015, pp. 2867–2873.

[12] J. Bruce, K. Caluwaerts, A. Iscen, A. P. Sabelhaus, and V. SunSpiral, "Design and evolution of a modular tensegrity robot platform," in *ICRA*, May 2014, pp. 3483–3489.

[13] Nasa tensegrity robotics toolkit (ntrt). [Online]. Available: http://ti.arc.nasa.gov/tech/asr/intelligent-robotics/tensegrity/ntrt/

[14] Bullet physics library. [Online]. Available: bulletphysics.org

[15] K. Caluwaerts, J. Despraz, A. Işçen, A. P. Sabelhaus, J. Bruce, B. Schrauwen, and V. SunSpiral, "Design and control of compliant tensegrity robots through simulation and hardware validation," *Journal of The Royal Society Interface*, vol. 11, no. 98, 2014. [Online]. Available: http://dx.doi.org/10.1098/rsif.2014.0520

[16] Ntrt model of ductt. [Online]. Available: https://github.com/NASA-Tensegrity-Robotics-Toolkit/NTRTsim/tree/DuCTT/src/dev/axydes/DuCTT

[17] H.-J. Schek, "The force density method for form finding and computation of general networks," *Computer Methods in Applied Mechanics and Engineering*, vol. 3, no. 1, pp. 115 – 134, 1974. [Online]. Available: http://www.sciencedirect.com/science/article/pii/0045782574900450